Volume-fraction dependence of elastic moduli and transition temperatures for colloidal silica gels

M. C. Grant and W. B. Russel

Department of Chemical Engineering, Princeton University, Princeton, New Jersey 08544-5263
(Received 23 October 1992)

Colloidal silica spheres bearing grafted octadecyl chains dispersed in hexadecane undergo a sol-gel transition with decreasing temperature. The gelation temperature depends on the volume fraction ϕ and, perhaps, the particle size. For $\phi > \phi_{gel}(T)$, the value at the transition, the elastic modulus varies as $(\phi - \phi_{gel})^s$ with the prefactor and exponent independent of temperature. This form resembles prediction from static percolation theories, but the exponent $s = 3.0 \pm 0.5$ lies significantly below those expected and the transition volume fraction varies with temperature. The relationship of the gelation transition to dynamic percolation and phase transitions predicted by equilibrium statistical mechanics has also been addressed. Matching the calculated structure factor for adhesive spheres with that measured by static light scattering yields the unknown strength of the interparticle attraction as a function of temperature. Though an imperfect fit introduces considerable uncertainty, this empirical relationship distinguishes the gel transition from both the dynamic percolation threshold and the spinodal associated with the fluid-fluid transition for adhesive spheres. Thus we conclude that gelation in this colloidal dispersion corresponds to a metastable state lying between the fluid-solid phase boundary and the spinodal.

PACS number(s): 64.70.−p, 82.70.Gg

I. INTRODUCTION

Colloidal dispersions undergo phase transitions similar to those for molecular systems. With purely repulsive potentials both nonaqueous [1] and aqueous [2] polymer lattices show a disorder-order transition for $0.5 \leq \phi < 0.55$ while dispersions of polymerically stabilized poly(methylmethacrylate) (PMMA) spheres exhibit the disordered-fluid to ordered-crystal and fluid glass transitions [3,4]. Likewise, silica spheres grafted with octadecyl chains in cyclohexane, which behave as hard spheres, rearrange themselves into an irridescent ordered phase when concentrated sufficiently slowly by gravity settling [5,6].

For the same octadecyl silica, changing the solvent and temperature alters the particle-particle interactions from repulsive to weakly or strongly attractive [7]. For example, dispersing the particles in benzene at high temperatures and then cooling produces weak attractions, causing spinodal decomposition [8,9] followed by separation into coexisting, though incompletely equilibrated, phases. Dispersing the particles in cyclohexane and adding free polystyrene also induces an attraction and phase separation [10]. In some cases, however, attractive interparticle potentials produce a macroscopically homogeneous gel [11] that can persist for extended periods in the absence of gravity or other forces driving consolidation. The distinction between systems that phase separate macroscopically and those forming persistent gels remains unclear.

For interpreting quantitatively the formation of colloidal gels, crystals, or coexisting phases due to short-range attractions of unknown form, Baxter's adhesive sphere [12],

$$\frac{\Phi(r)}{kT} = \lim_{d \to 2a} \begin{cases} \infty, & 0 < r < 2a \\ -\ln\dfrac{d}{12\tau(d-2a)}, & 2a < r < d \\ 0, & d < r , \end{cases} \quad (1)$$

defined such that

$$\lim_{d \to 2a} e^{-\Phi/kT} = H(r - 2a) + \frac{a}{6\tau}\delta(r - 2a) , \quad (2)$$

provides a convenient one-parameter (τ^{-1}) model. Here H is the Heaviside step function and δ is the Dirac δ function. This potential comprises a square well with infinite depth and zero width.

The phase diagram for adhesive spheres exhibits a first-order gas-liquid transition with the associated spinodal and a critical point at $\tau = 0.0976$ and $\phi = 0.1213$ [13,14]. In addition, Smithline and Haymet [15] identified, via the density-functional theory of freezing, a fluid-solid transition that converges to that for hard spheres as $\tau \to \infty$. Unfortunately, numerical difficulties confined their results to $\tau > 0.4$. Thus, one can only infer, by analogy with other work [16], that this fluid-solid transition, rather than the fluid-fluid one, determines the equilibrium transition over the full range of τ. Within the equilibrium fluid phase, particles still cluster at finite τ due to the attractions. Chiew and Glandt [17] derived the average cluster size as a function of volume fraction ϕ within the Percus-Yevick approximation and identified the dynamic percolation boundary $\tau_p(\phi)$ with the formation of an infinite cluster. Subsequent Monte Carlo simulations [18,19] refine the predictions of the percolation boundary, indicating an intersection with the binodal and spinodal at the critical point. Kranendonk and Frenkel [19] also extracted the radial distribution function $g(r)$ and its Fourier transform, the static structure factor $S(aq)$, from their simulations and found reasonable conformity with predictions from the analytical theory [20]. Thus the structure and phase behavior of the adhesive sphere model is sufficiently developed for interpreting observations with the octadecyl silica dispersions.

In the first such effort, de Kruif *et al.* [21] fit the predicted structure factor to small-angle neutron scattering from silica particles in benzene to quantify the increasing strength of the attraction with decreasing temperature. One should note, however, that the apparent τ^{-1} increases with increasing volume fraction and the calculated structure factors closely resemble those measured only at $\phi = 0.19$. Woutersen and de Kruif [22] measured the viscosity and the mutual diffusion coefficient, as well as the static structure factor via light scattering, at dilute volume fractions to demonstrate more conclusively that τ and the osmotic second viral coefficient ($A_2 = 4 - 1/\tau$) decrease rapidly below a critical temperature. The temperature dependence of the attraction resembles that expected from simple mean-field theories for interactions between grafted polymer layers in a poor solvent, i.e., $\Phi_m/kT = \alpha(\Theta/T - 1)$, with Θ the temperature at which the attraction vanishes and α a dimensionless constant.

Associated experiments with these dispersions demonstrate clearly that reducing the temperature until $\tau < 0.1$ will cause spinodal decomposition [9] and phase separation [8]. The $\tau(\phi)$ corresponding to the spinodal conforms nicely to that predicted, but the volume fractions ϕ_s of the separated dense phase deviate substantially from those expected for either the fluid-fluid or fluid-solid transitions. However, the magnitude and trend of $\phi_s(\tau)$ suggest an incompletely equilibrated solid phase arising from the latter. With a different solvent and/or stronger attractions, a gel forms with a fractal structure of dimension $d = 2.10 \pm 0.05$ independent of volume fraction [23].

For nonequilibrium structures such as colloidal gels, little theory is available. Static percolation theories, derived by randomly placing particles on a lattice, generally ignore correlations due to attractive forces. Consequently, they yield a threshold volume fraction ϕ_{gel} that depends on the nature, but not the magnitude, of the interparticle force and the coordination number of the lattice [24–27]. For isotropic forces the threshold coincides with that for conductivity, i.e., $\phi_{gel} = 0.14$ for a face-centered-cubic lattice, and the network is fractal with $d = 2.5$. Above the threshold, the shear modulus increases from zero according to $(\phi - \phi_{gel})^s$ with $s = 3.55 \pm 0.05$ [28]. An alternative theory, envisioning a network comprised of close-packed fractal clusters, leads to $\phi_{gel} = 0$ and $s = 3.5 \pm 0.2$ for clusters with $d = 1.75$ or $s = 4.5 \pm 0.5$ for $d = 1.98$ [29]. The different fractal dimensions correspond to different modes of aggregation. For example, clusters sticking irreversibly upon the first collision form relatively open aggregates of the first type [30], while clusters that stick only after a large number of contacts form the denser fractals [31].

In the following sections, we first discuss an alternative correlation of the shear moduli reported previously [32], motivated by the theory mentioned above. Then we compare the structure factors expected for adhesive spheres with those detected by static light scattering to estimate the strength of the attractions τ^{-1} as a function of temperature. Finally, from the strength of the interparticle attractions, we argue that the gel transition derives from the solid-liquid transition, rather than dynamic percolation, for adhesive spheres.
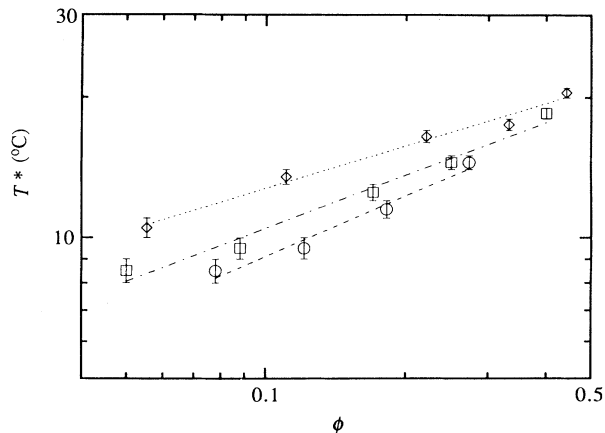

FIG. 1. $T^* = \beta\phi^\alpha$ for $a = 47$ nm ($\Diamond$), $a = 56$ nm ($\circ$), and $a = 72$ nm ($\square$).

II. ANALYSIS OF RHEOLOGICAL RESULTS

A. Identification of the gel transition

Rheological data [32] showed that octadecyl silica-hexadecane dispersions are fluids above a well-defined temperature and solids below, with the transition occurring over a 1 °C range. For each of the three particle sizes studied, the transition is best represented by

$$T^* = T_{gel} - 18 = \beta\phi^\kappa , \tag{3}$$

as shown in Fig. 1. Note that 18 °C is the freezing temperature of hexadecane. The empirical fitting parameters, given in Table I with standard deviations for each set of data, probably have no physical significance but are convenient for the analysis of experimental data in later sections.

B. Volume-fraction dependence of G'

Small-amplitude oscillatory measurements yielded elastic moduli at a particular temperature that vary with volume fraction roughly according to a power law. Since the elastic modulus decreases rapidly as the volume fraction approaches ϕ_{gel} and ϕ_{gel} increases with temperature, the apparent power-law index increases with temperature. Previously [32] we attributed this to structural changes with temperature, although static light-scattering results demonstrate the fractal dimension to be independent of temperature and volume fraction. This and the prediction from static percolation theory indicate that the relevant feature of the microstructure is the dis-

TABLE I. Results of power-law fits for the gel-transition data.

a (nm)	β (°C)	κ
47	25.7 ± 1.0	0.30 ± 0.02
56	24.5 ± 2.6	0.43 ± 0.05
72	25.0 ± 1.7	0.38 ± 0.03

TABLE II. Critical gelation volume fraction $\phi_{gel}(T)$ at several temperatures for each sample.

a (nm)	Temp. 20 °C	22 °C	24 °C	26 °C
47	0.000	0.002	0.008	0.021
56	0.003	0.015	0.038	0.074
72	0.001	0.008	0.023	0.049

tance from the gel transition, suggesting the scaling

$$G' = G'_0 [\phi - \phi_{gel}(T)]^s . \tag{4}$$

For this purpose, values for $\phi_{gel}(T)$ for each system (Table II) were calculated by extrapolating the empirical correlation (3) to the temperatures of the rheological experiments.

Replotting the elastic moduli as G' versus ϕ^* $[=\phi - \phi_{gel}(T)]$ and excluding the points for $\phi^* \approx 0$ eliminates the strong temperature dependence, in agreement with the static light-scattering results. Figures 2 and 3, with different symbols indicating data at different temperatures, show that data for $a = 56$ and 72 nm all collapse onto straight lines, as expected from (4). Figure 4 for $a = 47$ nm, however, shows a temperature dependence for $0.1 < \phi^* \approx \phi < 0.3$, leaving the normalization less effective. This residual temperature dependence may result from the uncertainties in the extrapolated $\phi_{gel}(T)$ or some inadequacies in the $a = 47$ nm data, the first set taken. This does not obscure, however, the striking conclusion that the prefactor G'_0, characterizing the elasticity of the interparticle bonds, and s, characterizing the structure, are both independent of temperature.

The values for G'_0 and s extracted from the data (Table III) differ among the three batches of particles; however, the range of radii is too narrow to ascribe this to a dependence on particle size. A variation in graft density, or some other feature of the octadecyl layer, is equally possible. Nonetheless, the power-law indices, 3.0 ± 0.5, are consistent with experimental results on other systems
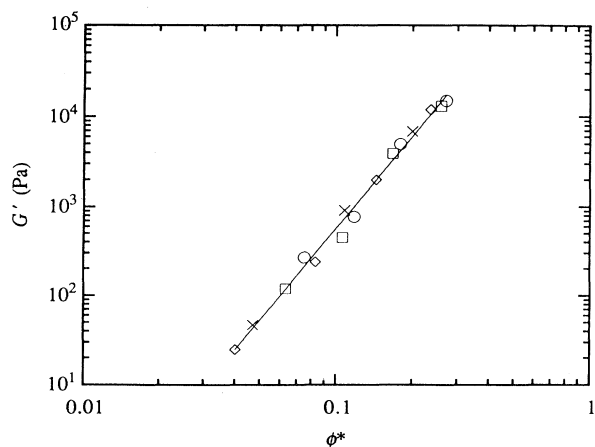

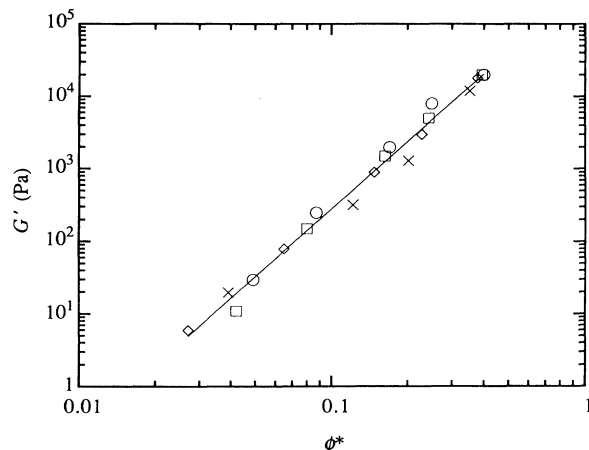FIG. 3. Superposition of elastic moduli for $a = 72$ nm at temperatures of 20° C (○), 22 °C (□), 24 °C (◇), and 26 °C (×) and power-law fit (——).

[29,32–34], though outside the range expected from static percolation or the existing fractal theory.

III. ANALYSIS OF STATIC LIGHT SCATTERING

A. Structure factor for adhesive spheres

Within the equilibrium fluid region of the phase diagram, the static structure, generally characterized by the radial distribution function $g(r)$, depends on the volume fraction ϕ and the adhesion parameter τ. The Fourier transform of $g(r)$ comprises the static structure factor $S(aq)$, which is detectable by static light scattering, provided either the refractive index difference between particles and fluid or the volume fraction of particles is small enough to avoid multiple scattering. For the octadecyl silica-cyclohexane dispersions the optical match suffices for measurements over a broad range of concentrations for particles smaller than 100 nm. The poorer match in
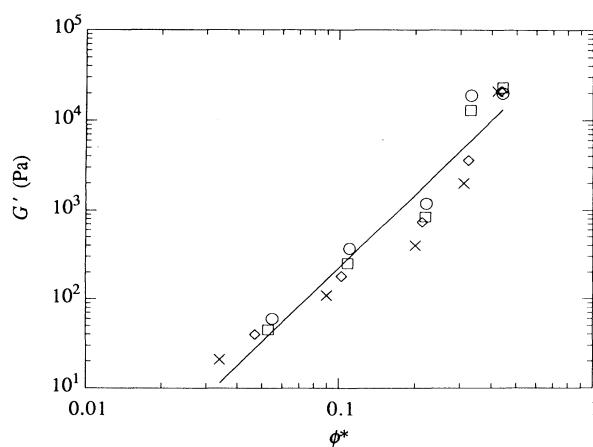

FIG. 2. Superposition of elastic moduli for $a = 56$ nm at temperatures of 20 °C (○), 22 °C (□), 24 °C (◇), and 26 °C (×) and power-law fit (——).

FIG. 4. Superposition of elastic moduli for $a = 47$ nm at temperatures of 20 °C (○), 22 °C (□), 24 °C (◇), and 26 °C (×) and power-law fit (——).

TABLE III. Results of power-law fit for modulus below the gel transition.

a (nm)	G_0' (Pa)	s
47	$(1.25\pm0.55)\times10^5$	2.75 ± 0.19
56	$(1.50\pm0.33)\times10^6$	3.42 ± 0.09
72	$(3.51\pm0.72)\times10^5$	3.09 ± 0.08

hexadecane limits the range of the experiment. Nonetheless, one can still detect the structure under conditions affected significantly by the attraction and compare with theoretical predictions to estimate τ.

The fractorization of Baxter [12] represents the static structure factor as the product of two terms:

$$S(aq)=[Q(aq)Q(-aq)]^{-1} , \tag{5}$$

where

$$Q(aq)=1-2\pi\rho\int_0^\infty Q(r)\frac{\sin qr}{qr}dr . \tag{6}$$

Here a is the radius, ρ is the number density, r is the center-to-center distance, $q=(4\pi n_0/\lambda_0)\sin(\theta/2)$, n_0 is the index of refraction of solvent, λ_0 is the wavelength of the incident light, and θ is the forward-scattering angle. When $r>2a$, $Q(r)=0$. For $r\leq2a$, $Q(r)$ is a quadratic function of r:

$$Q(r)=Ar^2+Br+C , \tag{7}$$

with coefficients [20]

$$A=0.5(1+2\phi-\mu)(1-\phi)^{-2} ,$$

$$B=a(-3\phi+\mu)(1-\phi)^{-2} ,$$

$$C=-4a^2A-2aB+a^2\lambda/3 ,$$

where $\mu=\lambda\phi(1-\phi)$ and

$$\lambda=\frac{6}{\phi}\left\{\left[\tau+\frac{\phi}{1-\phi}\right]\right.$$
$$\left.-\left[\left[\tau+\frac{\phi}{1-\phi}\right]^2-\frac{\phi(2+\phi)}{6(1-\phi)^2}\right]^{1/2}\right\} . \tag{8}$$

Note that λ is real provided

$$\left[\frac{\phi}{1-\phi}+\tau\right]^2-\frac{\phi(2+\phi)}{6(1-\phi)^2}\geq0 . \tag{9}$$

For dilute solutions, Eq. (8) becomes

$$\lambda=\frac{1}{\tau}+\left[\frac{5}{2\tau}-\frac{1}{\tau^2}+\frac{1}{12\tau^3}\right]\phi$$
$$+\left[\frac{4}{\tau}-\frac{1}{2\tau^2}-\frac{1}{12\tau^3}\right]\phi^2+\cdots . \tag{10}$$

Regnaut and Ravey [20] proceed by expressing the structure factor analytically as

$$S^{-1}(aq)=\left[1-12\phi\left[AI_2(u)+\frac{B}{2a}I_1(u)+\frac{C}{4a^2}I_0(u)\right]\right]^2$$
$$+\left[12\phi\left[AJ_2(u)+\frac{B}{2a}J_1(u)\right.\right.$$
$$\left.\left.+\frac{C}{4a^2}J_0(u)\right]\right]^2 , \tag{11}$$

with $u=2aq$,

$$I_n(u)=\int_0^1 x^n\cos ux\, dx ,$$

and

$$J_n(u)=\int_0^1 x^n\sin ux\, dx ,$$

and integrating by parts to obtain

$$S^{-1}(aq)=\left[1-\frac{12\phi}{u^3}\left[2A(u\cos u-\sin u)+\frac{B}{2a}u(\cos u-1)+\frac{\lambda u^2}{12}\sin u\right]\right]^2$$
$$+\left\{\frac{12\phi}{u^3}\left[2A\left[u\sin u+\cos u-1-\frac{u^2}{2}\right]+\frac{B}{2a}u(\sin u-u)+\frac{\lambda u^2}{12}(1-\cos u)\right]\right\}^2 . \tag{12}$$

Several limiting cases follow directly. When $\tau^{-1}=0$, $S(aq)$ reproduces the results for hard spheres. In the limit of zero scattering angle $(q=0)$, Eq. (10) reduces to

$$S^{-1}(0)=[1+(8A+3B/a-\lambda)\phi]^2 . \tag{13}$$

For $\phi\ll1$, the structure factor simplifies further to

$$S^{-1}(0)=\frac{1}{kT}\frac{\partial\pi}{\partial\rho}$$
$$=S_{HS}^{-1}(0)-\frac{2\phi}{\tau}-\left[\frac{15}{\tau}-\frac{3}{\tau^2}+\frac{1}{6\tau^3}\right]\phi^2+O(\phi^3) , \tag{14}$$

with the hard-sphere structure factor as

$$S_{HS}^{-1}(0)=1+8\phi+30\phi^2+\cdots . \tag{15}$$

B. Physically acceptable solutions for the PY equation

Baxter [12] and Watts, Henderson, and Baxter [13] noted three conditions that must be satisfied by physically acceptable solutions of the Percus-Yevick (PY) equation:

(i) The parameter λ must be real, which means remaining below the curve

$$\tau^{-1} = \frac{1-\phi}{\left[\left[\frac{\phi(2+\phi)}{6}\right]^{1/2} - \phi\right]} \qquad (16)$$

in the (τ^{-1}, ϕ) plane.

(ii) The compressibility,

$$kT\left[\frac{\partial\rho}{\partial\pi}\right]_T = 1 + 4\pi\rho\int_0^\infty r^2[g(r)-1]dr , \qquad (17)$$

must be finite, excluding all points within the spinodal curve emanating from the critical point at $\phi_c = 0.1213$ and $\tau_c = 0.0976$.

(iii) The integral in (17) must be absolutely convergent, which requires $\mu < 1 + 2\phi$ or

$$\lambda < \frac{1+2\phi}{\phi(1-\phi)} , \qquad (18)$$

Figure 5 depicts these three constraints with Eqs. (16) and (17), the lighter and darker solid curves, respectively, coinciding for $\phi < \phi_c = 0.1213$ and (18), the dashed curve, coinciding with (17) for $\phi > \phi_c$. Thus Eq. (16) proves irrelevant, since it lies on the spinodal for $\phi < \phi_c$ and within it for $\phi > \phi_c$. So only the τ^{-1} and ϕ pairs lying outside the spinodal and below Eq. (18) comprise physically acceptable solutions.

Figure 6 illustrates some important features of the structure factors for adhesive spheres with $\tau = 0.10$, just above the critical point, and volume fractions in the range of our experimental data. For $\phi \leq 0.01$, $S(aq) \approx 1$. With increasing volume fraction, $S(0)$ increases because of the attraction, but the curves also decrease faster with increasing aq and cross $S(aq) = 1$ at decreasing values of aq. For all volume fractions, $S(aq)$ reaches a minimum

FIG. 6. Calculated structure for $\tau^{-1} = 10$ at several volume fractions.

at $aq \approx 2$ and oscillates about unity at larger aq. The first peak of $S(aq)$ for hard spheres appears at $aq \approx \pi$ but, for adhesive spheres, is shifted slightly to the right, to $aq \approx 4$. Figure 7, depicting $S(0)$ as a function of τ^{-1} for a similar range of volume fractions, demonstrates an insensitivity of $S(0)$ to τ^{-1} for $\phi \leq 0.01$ over the full range of interest. Therefore, experiments designed to extract τ^{-1} must be performed at $\phi > 0.05$.

C. Strength of the attraction from $S(aq)$

The structure factors from our static light-scattering data show high sensitivity to temperature, implying a strong variation in the strength of the attraction τ^{-1}. The data [32] pertain to silica-hexadecane dispersions of $\phi = 0.008$, 0.016, 0.032, 0.064, 0.085, and 0.113 at several temperatures from 25 to 55 °C, with the volume fraction calculated from the weight concentration through the particle density in the dispersion (1.47 g/ml) rather than the dry particle density (1.70 g/ml) as reported previously. The structure factors were measured immediately after equilibrating the samples at the specified temperatures and did not change during the experiment.

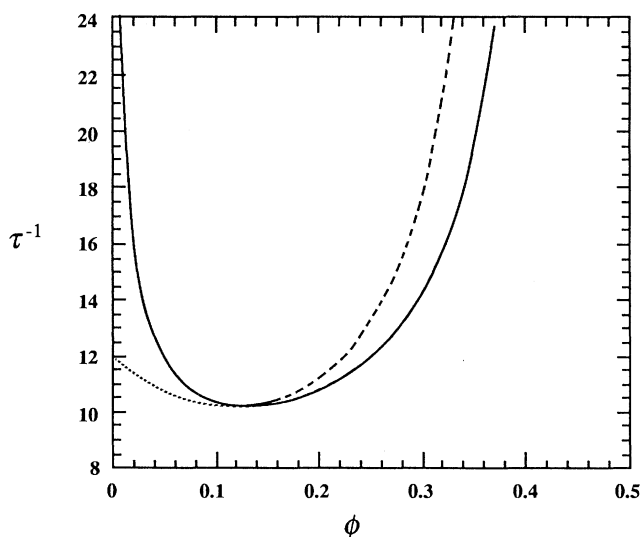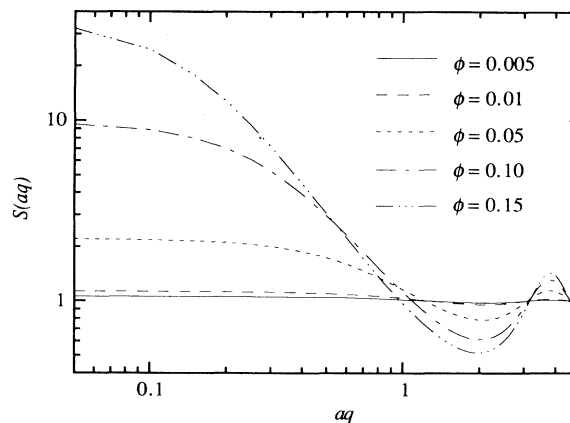Three factors complicate the estimation of τ^{-1} from

FIG. 5. Points above the solid curve and on the dashed curve correspond to physically unacceptable solutions of the PY equation. ——, locus of points where $S(0)$ diverges; . . ., for $\lambda = (1+2\phi)/[\phi(1-\phi)]$; — — —, τ^{-1} for real λ.
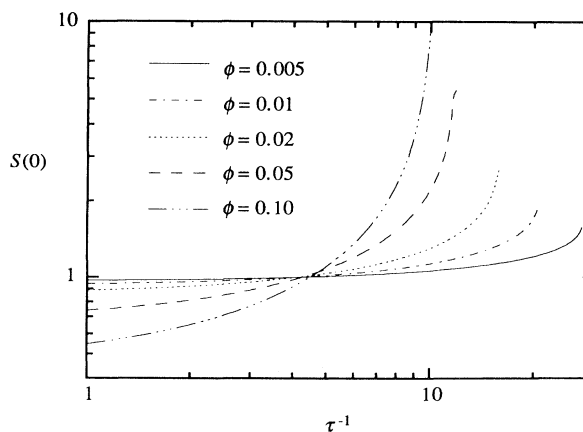

FIG. 7. Calculated $S(0)$ at several volume fractions.

quantitative comparison with the predictions in the previous section:

(i) Even at high temperatures, or in a good solvent such as cyclohexane, the static structure factor for $\phi \ll 1$ rises above unity at low q [e.g., $S(0)-1=0.1-0.3$], implying the presence of some permanent aggregates.

(ii) The calculated structure factors for adhesive spheres with $\phi < 0.05$ are insensitive to the strength of the attraction for $\tau^{-1} < 20$ (Fig. 6), necessitating an unrealistically strong attraction to account for modest values of $S(0)-1$ in the measurements (Fig. 7).

(iii) Since hexadecane matches rather poorly the refractive index of the silica spheres, multiple scattering becomes significant for $\phi > 0.12$, limiting the range of scattering measurements.

To minimize the effect of permanent aggregates, we treat the Rayleigh ratio $R(aq)$ in hexadecane at 55 °C as a particle form factor and normalize the data accordingly, defining

$$\bar{S}(aq)=\delta n [R(aq)][R(aq)]_{55\,°C}^{-1} , \qquad (19)$$

with δn accounting for the ratio of the refractive index difference at the prescribed temperature to that at 55 °C. Due to (ii) and (iii), no meaningful analysis is possible for $\phi < 0.05$ or > 0.12. In addition, some of the scattering curves for $T \leq 30$ °C detect a fractal structure associated with gelation [23], which lies beyond the validity of the Percus-Yevick equation. So in the following, we estimate τ^{-1} by matching the calculated structure factor with data for $\phi = 0.064, 0.085$, and 0.113 at $T \geq 33$ °C.

The strength of the attraction is derived by fitting Eq. (12) to the data using τ^{-1} and δn as fitting parameters. Figures 8–10 illustrate the quality of the fit for several temperatures and volume fractions. At 33 °C (Fig. 8), the calculated and measured $S(aq)$ agree well for each volume fraction, especially for $\phi = 0.085$ with $\tau^{-1}=9.8$. Similarly, at 35 °C (Fig. 9), the calculated $S(aq)$ closely resemble those from experiments, particularly for $\phi = 0.113$ with $\tau^{-1}=8.4$, and suggest a reduced attraction relative to 33 °C. Increasing temperature further weakens the attraction and decreases the magnitude of $S(0)-1$, but the computed curves, e.g., for 38 °C with
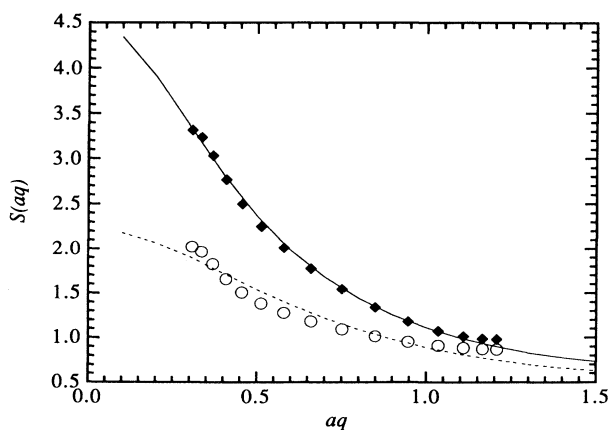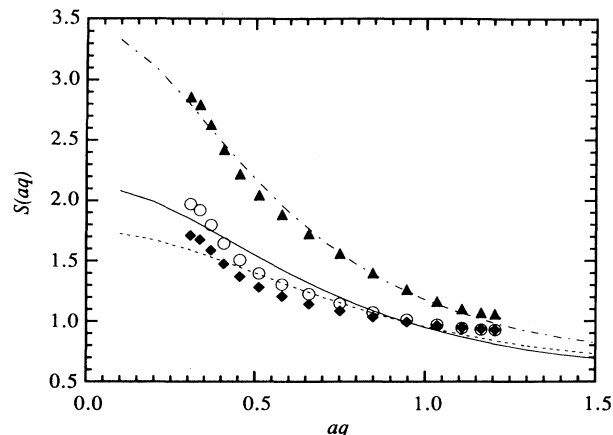

FIG. 9. Best fit for static light-scattering data at 35 °C and $\phi = 0.064$ (♦), $\phi = 0.085$ (○), and $\phi = 0.113$ (▲).

$\tau^{-1} \approx 8$ (Fig. 10), fit the data rather poorly. The situation at temperatures of 40–50 °C is qualitatively similar, with the computed curves consistently failing to reproduce sharp upturns of the data at $aq \sim 0.5$ but dealing well with highly correlated structures at higher volume fractions and aq. This clearly suggests either an inability of the theory to handle large aggregates or a problem with the data at small scattering angles, but we have not determined which.

Table IV summarizes the best-fit values of τ^{-1}. The $\pm$ values represent deviations from fitting the $aq \leq 0.5$ and > 0.5 portions of the scattering curves, respectively. For example (Fig. 11), for $\phi = 0.064$ and 0.085 at 38 °C, the data at wider angles provide lower bounds of 5.2 and 5.6, while data at the lower angles yield upper bounds of 10.3 and 9.7. Figure 12, based on the mean values from Table IV, establishes clearly that all points fall below the solid and dashed curves and correspond, therefore, to physically acceptable solutions of the Percus-Yevick equation.

Plotting the resulting strength of attraction as a function of temperature (Fig. 13), with error bars indicating the deviations resulting from fitting different portions of
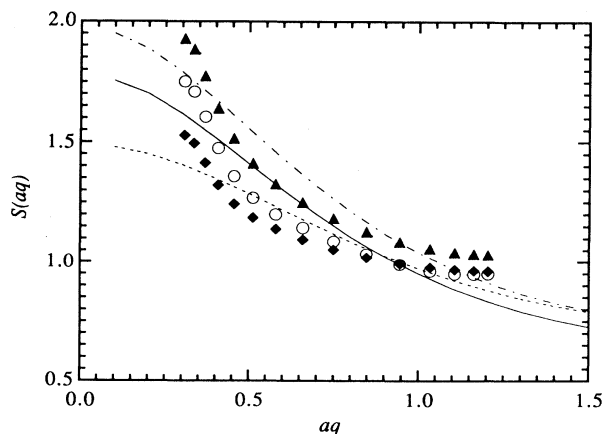

FIG. 8. Best fit for static light-scattering data at 33 °C and $\phi = 0.064$ (♦) and $\phi = 0.085$ (○).

FIG. 10. Best fit for static light-scattering data at 38 °C and $\phi = 0.064$ (♦), $\phi = 0.085$ (○), and $\phi = 0.113$ (▲).

TABLE IV. Best fit τ^{-1} at several temperatures and volume fractions.

T (°C)	τ^{-1}		
	$\phi = 0.064$	$\phi = 0.085$	$\phi = 0.113$
33	$9.9 + 0.9$ -2.0	$9.8 + 0.1$ -0.3	
35	$8.7 + 1.8$ -2.3	$8.5 + 1.3$ -1.8	$8.4 + 0.6$ -0.5
38	$7.6 + 2.7$ -2.4	$7.6 + 2.1$ -2.0	$7.1 + 1.8$ -1.9
40	$7.2 + 2.6$ -1.8	$6.8 + 2.1$ -1.5	$6.9 + 1.8$ -1.7
45	$5.6 + 2.9$ -1.3	$5.0 + 2.7$ -1.0	$5.0 + 2.4$ -1.1
50	$4.1 + 1.5$ -0.5	$4.2 + 1.4$ -0.4	$4.0 + 1.7$ -0.4

FIG. 12. Data from the best fits and the curves are from Fig. 1 at temperatures of 33 °C (○), 35 °C (●), 38 °C (◇), 40 °C (◆), 45 °C (△), and 50 °C (▲).

the scattering curves, indicates that τ^{-1} decreases roughly linearly with increasing temperature (C) following

$$\tau^{-1} = (18.5 \pm 1.4) - (0.285 \pm 0.035)T . \qquad (20)$$

The uncertainties are standard deviations from a linear regression of the best-fit parameters including those from the upper and lower portions of the scattering curves. Within the relatively narrow range of temperatures of interest, (20) establishes the sought-after connection between temperature and interparticle potential, suggesting that the attraction only disappears for $T > 340$ K.

One can devise other schemes for estimating τ^{-1} from the data as well. For example, extrapolating, albeit roughly, $S(aq)$ to $aq = 0$ and then plotting $[S^{-1}(0) - S_{HS}^{-1}(0)]/\phi S_{HS}^{-1}(0)$ against ϕ yields τ^{-1} from either the slope or intercept according to (14). Both values fall within the error bounds noted in Table IV. So we conclude that the bounds assess realistically the uncertainty arising from the curve fitting as well as the normalization (19).
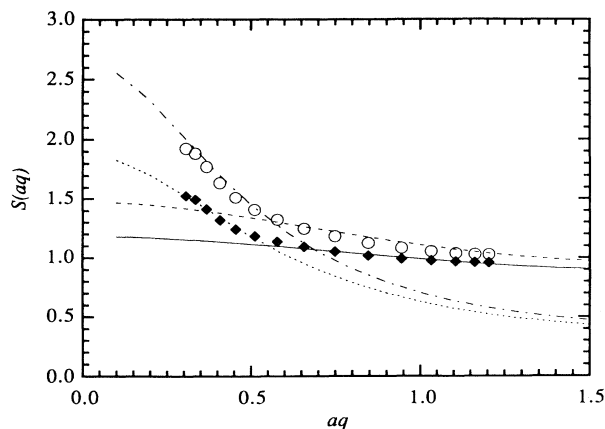
A comparison with similar characterizations of other systems is worthwhile. For octadecyl silicas in benzene and dodecane, Rouw, Vrij, and Kruif [35] performed light-scattering measurements to extract τ^{-1} as a function of temperature. Static light scattering, actually turbidity, yielded the apparent second virial coefficient as a function of wavelength, permitting the true value to be obtained from the intercept at infinite wavelength. In this way they found τ^{-1} to increase with decreasing temperature, as illustrated in Fig. 13. The coincidence of the data above 310 K is surprising in view of the disparate behavior in the two solvents. However, gelation in dodecane and phase separation in benzene appear at lower temperature, where values for τ^{-1} extracted from dynamic light-scattering measurements (not shown here) differ significantly. Our measurements in hexadecane indicate substantially stronger attraction but a similar temperature dependence to that observed with dodecane.

FIG. 11. Best fits for the upper and the lower portions of scattering curves at 38 °C with $\phi = 0.064$ (◆) and $\phi = 0.113$ (○).

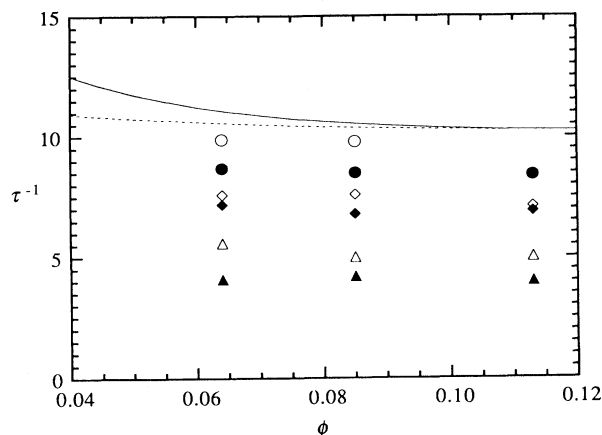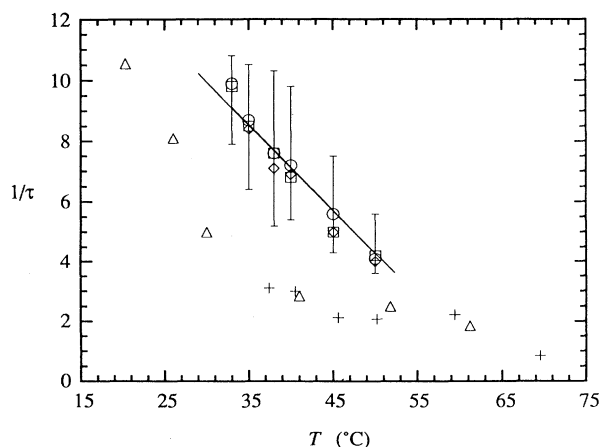FIG. 13. Strength of the attraction as a function of temperature in hexadecane for $\phi = 0.064$ (○), $\phi = 0.085$ (□), and $\phi = 0.113$ (◇) with (———) $\tau^{-1} = (18.5 \pm 1.43)$ $- (0.285 \pm 0.0348)T$ and in benzene (△) and dodecane (+) from [35].

IV. INTERPRETATION OF THE GEL TRANSITION

Both rheological and static light-scattering measurements reveal a sharp transition from a fluid dispersion to a macroscopically uniform gel with no observed phase separation. At a constant temperature, these silica gels consolidate under gravity over a period of a few days to weeks, leaving a clear supernatant and a thicker gel. This suggests that when gravitational forces exceed the yield stress, the particles within the gel rearrange on a much longer time scale than our experiment. The consolidation occurs much faster at low volume fractions, implying a faster rearrangement in a looser network than in a more compact gel. Consolidation can be prevented by placing the sample on a mixing roller, thereby reducing the effect of gravity. Then a sample that normally consolidates in less than a day neither consolidates nor phase separates for over a month. This suggests that these octadecyl silica-hexadecane gels at conditions well into the two-phase region do not phase separate but will, over time, become more compact under gravity.

The question remains whether the observed transition corresponds to the dynamic percolation threshold, the spinodal, or the solid-liquid transition in the phase diagram for adhesive spheres. Previously, we estimated the strength of the attraction (τ^{-1}) under the assumption that the gel transition corresponded to the percolation threshold [32]. With the strength of the attraction now estimated from the static structure factors, that assumption can be relaxed.

The task is to transfer the measured gel transition onto the τ-ϕ phase diagram. Although the static light-scattering measurements were at conditions within the fluid region of the phase diagram, the resulting relationship for $\tau^{-1}(T_{gel})$ is generally valid. Thus substituting T_{gel} for $a = 47$ nm from (3) into (20) gives

$$\tau_g^{-1} = (13.4 \pm 1.6) - (7.3 \pm 1.0)\phi^{0.30 \pm 0.02} , \qquad (21)$$

with the uncertainties from a first-order analysis of the propagation of error (Ref. [36], p. 45).

The calculated points in Fig. 14 correspond to the measured points on the gel transition diagram (Fig. 1) with the relative error in τ_g the same as that for τ_g^{-1}. Clearly, the gel transition overlaps both the dynamic percolation threshold and the spinodal curve at volume fractions below the critical point $(\phi < 0.15)$. But for $\phi \geq 0.20$, the gelation occurs well below the percolation line and significantly above the spinodal. For $\phi > 0.5$, it is not clear whether the silica gel transition sweeps up parallel to the liquid-solid transition predicted by Smith and Haymet [15]. Despite the uncertainty, this strongly suggests a metastable state between the fluid-solid phase boundary and the spinodal. Hence, we conclude that this gelation phenomenon arises from the nucleation and growth of clusters in the metastable region beyond a fluid-solid transition but short of the spinodal. Our light-scattering measurements reported previously [32] indicate a fractal structure for these clusters.

Another intriguing issue is the disparate behavior of the octadecyl silica spheres in benzene and hexadecane. Macroscopic phase separation occurs in benzene on a
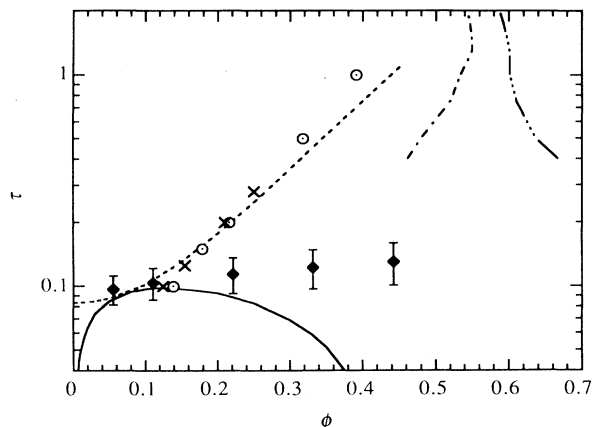

FIG. 14. Phase diagram for adhesive spheres including the gel transition for silica-hexadecane dispersions: ——, spinodal; (⊙), percolation (Kranedonk and Frenkel, 1988); ×, percolation (Seaton and Glandt, 1987); — — —, percolation (Chiew and Glandt, 1983); —·—·—, freezing (Smithline and Haymet, 1985); —·—·—, melting (Smithline and Haymet, 1985); ◆, silica-hexadecane gel transition.

reasonable time scale, though full equilibrium remains difficult to achieve, but in hexadecane gels persist indefinitely in the absence of gravitational consolidation. Arguments for a different mechanism for the attraction [37], a coordinated freezing of octadecyl and hexadecane chains in the gap between particles, suggest different dynamics as well. Consider, for example, the characteristic time for doublet breakup, an essential step in the relaxation from a gel to a condensed phase. For adhesive spheres surrounded by pure solvent, the mobility for relative motion decreases linearly with the separation, vanishing at contact. Consequently, the time scale diverges logarithmically as the range of the attraction goes to zero; nonetheless, for particles and grafted layers of the size considered here and attractions in the vicinity of gelation, equilibration still should be reasonably rapid. However, the mobility of particles interacting within the attractive well may be substantially reduced by interpenetration of the grafted layers or the freezing process mentioned above. So the possibility exists for dramatically longer time scales, depending on the mobility of the solvent in the gap. This might bear on the difference in the macroscopic behavior in hexadecane relative to that in benzene.

V. SUMMARY

In this paper we have tried to establish two points: (i) the scaling of the shear modulus of the gel as $G' = G_0'[\phi - \phi_g(T)]^{3.0 \pm 0.5}$; and (ii) the positioning of the gelation transition within the metastable region between the fluid-solid phase boundary and the spinodal. Neither argument is completely unassailable, though we think both have considerable merit. In addition, we suggest that the gelation in hexadecane, rather than the phase separation in benzene, arises from different dynamics between particles at small separations.

The correlation (i), motivated by the predictions from

static percolation theories, captures the temperature dependence of the shear modulus for each particle size and/or batch entirely within the threshold volume fraction. However, the prefactor varies substantially among the three batches of particles and exceeds the expected interparticle force per unit area $\Phi_m / \pi a^2 L \approx 10^3 - 10^4$ Pa, by a couple of orders of magnitude. Of course, the dependence of ϕ_g on the temperature and the value of the exponent are not predicted by any existing theory.

The uncertainty in the case for (ii) lies in the mediocre fit of the static structure factors to predictions from the adhesive sphere model. Rouw and de Kruif [23] and Rouw, Vrij, and de Kruif [35] encountered a similar difficulty as well; the dilute measurements of Woutersen and de Kruif [22] effectively ignore the issue by focusing on an integral property. Certainly, more definitive measurements for the octadecyl silica-hexadecane system would be preferable. However, complementary means of detecting the dynamic percolation transition [38] may resolve the question.

ACKNOWLEDGMENTS

[1] A. Kose and S. Hachisu, J. Colloid Interface Sci. **46**, 460 (1974)

[2] S. Hachisu and Y. Kobayashi, J. Colloid Interface Sci. **46**, 470 (1974).

[3] P. N. Pusey and W. van Megen, Nature **320**, 340 (1986).

[4] P. N. Pusey and W. van Megen, Phys. Rev. Lett. **59**, 2083 (1987).

[5] K. E. Davis, W. B. Russel, and W. J. Glantschnig, Science **245**, 507 (1989).

[6] C. Smits, W. J. Briels, J. K. G. Dhont, and H. N. W. Lekkerkerker, Prog. Colloid Polym. Sci. **79**, 287 (1989).

[7] J. W. Jansen, C. G. de Kriuf, and A. Vrij, J. Colloid Interface Sci. **114**, 471 (1986); **114**, 481 (1986); **114**, 492 (1986).

[8] P. W. Rouw, A. T. J. M. Woutersen, B. J. Ackerson, and C. G. de Kruif, Physica A **156**, 876 (1989).

[9] A. Vrij, M. H. G. M. Penders, P. W. Rouw, C. G. de Kruif, J. K. G. Dhont, C. S. Smits, and H. N. W. Lekkerkerker, Faraday Discuss. Chem. Soc. **90**, 31 (1990).

[10] H. De Hek and A. Vrij, J. Colloid Interface Sci. **84**, 409 (1981).

[11] P. D. Patel and W. B. Russel, J. Colloid Interface Sci. **131**, 192 (1989).

[12] R. J. Baxter, J. Chem. Phys. **49**, 2770 (1968).

[13] R. O. Watts, D. Henderson, and R. J. Baxter, Adv. Chem. Phys. **21**, 421 (1971).

[14] B. Barboy, J. Chem. Phys. **61**, 3194 (1974).

[15] S. J. Smithline and A. D. J. Haymet, J. Chem. Phys. **83**, 4103 (1985).

[16] A. P. Gast, C. K. Hall, and W. B. Russel, J. Colloid Interface Sci. **96**, 251 (1983); Faraday Discuss. Chem. Soc. **76**, 189 (1983).

[17] Y. C. Chiew and E. D. Glandt, J. Phys. A **16**, 2599 (1983).

[18] N. A. Seaton and E. D. Glandt, J. Chem. Phys. **86**, 4668 (1987).

[19] W. G. T. Kranendonk and D. Frenkel, Mol. Phys. **64**, 403 (1988).

[20] C. Regnaut and J. C. Ravey, J. Chem. Phys. **91**, 1211 (1989); **92**, 3250 (1990).

[21] C. G. de Kruif, P. W. Rouw, W. J. Briels, M. H. G. Duits, A. Vrij, and R. P. May, Langmuir **5**, 422 (1989).

[22] A. T. J. M. Woutersen and C. G. de Kruif, J. Chem. Phys. **94**, 5739 (1991).

[23] P. W. Rouw and C. G. de Kruif, Phys. Rev. A **39**, 5399 (1989).

[24] Y. Kantor, in *Scaling Phenomena in Disordered Systems*, edited by R. Pynn, and Skjeltorp (Plenum, New York, 1985).

[25] S. C. Feng and P. Sen, Phys. Rev. Lett. **52**, 216 (1984).

[26] Y. Kantor and I. Webman, Phys. Rev. Lett. **52**, 1891 (1984).

[27] S. C. Feng, P. N. Sen, B. I. Halperin, and C. J. Lobb, Phys. Rev. B **30**, 5386 (1984).

[28] S. C. Feng and M. Sahimi, Phys. Rev. B **31**, 1671 (1985).

[29] R. Buscall, P. D. A. Mills, J. W. Goodwin, and D. W. Lawson, J. Chem. Soc. Faraday Trans. I **84**, 4249 (1988).

[30] P. Meakin, J. Colloid Interface Sci. **102**, 491 (1984).

[31] R. Jullien and M. Kolb, J. Phys. A **17**, L639 (1984).

[32] M. Chen and W. B. Russel, J. Colloid Interface Sci. **141**, 564 (1990).

[33] R. Buscall and I. J. McGowan, Faraday Discuss. Chem. Soc. **76**, 277 (1983).

[34] Y. Otsubo, Langmiur **6**, 114 (1990).

[35] P. W. Rouw, A. Vrij, and C. G. de Kruif, Prog. Colloid Polym. Sci. **76**, 1 (1988).

[36] J. P. Holman, *Experimental Methods for Engineers*, 3rd ed. (McGraw-Hill, New York, 1978).

[37] C. G. de Kruif and J. C. Van Miltenburg, J. Chem. Phys. **93**, 6865 (1990).

[38] A. T. J. M. Woutersen, J. Mellema, C. Blom, and C. G. de Kruif (unpublished).